THE JOURNAL OF PHYSICAL CHEMISTRY C

Article

pubs.acs.org/JPCC

Calculation of TiO_2 Surface and Subsurface Oxygen Vacancy by the Screened Exchange Functional

Hongfei Li, Yuzheng Guo,* and John Robertson

Department of Engineering, Cambridge University, Cambridge CB2 1PZ, United Kingdom

ABSTRACT: The formation energies of oxygen vacancies at different surface and subsurface sites of anatase (101), anatase (001), and rutile (110) surfaces are calculated by the screened-exchange (sX) hybrid functional method. Our results show that the oxygen vacancy is more stable on the surface than subsurface for rutile (110), while it is a more stable subsurface than on the surface for anatase surfaces. These results are similar to those found by simple density functional theory, but now the sX hybrid functional gives the correct defect localizations. The defects introduce a gap state near the conduction band edge. For the most stable oxygen vacancy site at each TiO_2 surface, the +2 charge state dominates over a wide range of Fermi energies.

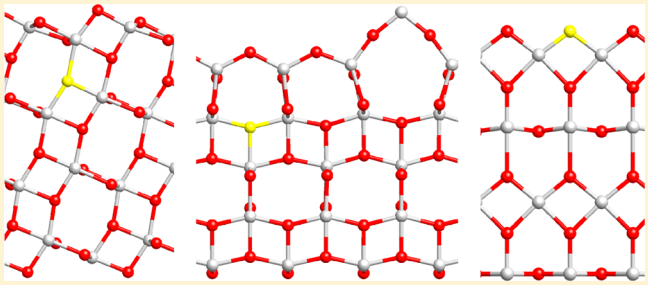

INTRODUCTION

Titanium oxide (TiO_2) is a technologically important transition metal oxide[1] widely used in photocatalysis,[2] solar energy conversion,[3] environmental cleanup,[4] and may be in future resistive random-access memories (RRAMs).[4] The oxygen vacancy (V_O) is the most important point defect in TiO_2, and it plays a crucial role in these applications. Electron bombardment results confirm that oxygen vacancies rather than Ti interstitials make the dominant contribution to the band gap states of TiO_2 surface.[5] Oxygen vacancies also influence the absorption of water and other molecules on TiO_2 surfaces in photocatalytic devices.[6] Similarly, oxygen vacancies form a conductive filament across the TiO_2 film in RRAM devices.[4,7,8] In addition, the oxygen vacancy usually forms at the surface region of TiO_2 in experiments, so the surface defects are more important than bulk ones.[9,10] Therefore, it is of great significance to understand the behavior of oxygen vacancies at TiO_2 surfaces and associate it with the behavior of TiO_2 surfaces and devices.

While rutile is the thermodynamically most stable bulk phase of TiO_2, anatase is more stable for particles below ~14 nm in size due to its lower surface energies.[11] Thus, anatase is more relevant to catalytic applications. There has been a continuing interest in the properties of anatase and rutile surfaces.[1] Rutile (110), its most stable surface, has a high surface energy (0.82J/m^2), whereas anatase has a much lower surface energy of 0.44J/m^2 for its most stable (101) facet. The more reactive (001) facet of anatase is calculated to have a surface energy of ~0.90 J/m^2. However, this surface can undergo a surface reconstruction to give the ad-molecule (ADM) reconstruction, as confirmed by STM,[12] with a calculated surface energy of 0.51 J/m^2. This minority TiO_2 facet has aroused much attention since it was fabricated by stabilizing with a hydrofluoric acid morphology controlling agent.[13]

As O vacancies mediate the reactivity of TiO_2 surfaces, it is expected that the surface with the higher vacancy concentration might be the most reactive. However, resonant photoemisssion experiments[14] suggest that anatase has a relatively low vacancy concentration. Cheng and Selloni[15] explained this by showing that the O vacancy is more stable subsurface in anatase, whereas it is more stable on the surface in rutile. Nevertheless, these results were obtained by the simple generalized gradient approximation (GGA) version of density functional theory with rather small supercells. It is well-known that local functionals such as GGA underestimate the band gap in semiconductors and insulators and do not handle the Coulomb interaction in strongly correlated systems well.[16,17] In TiO_2, this has the effect that local functionals underestimate the *d* electron localization and the amount of lattice distortions at vacancies. They underestimate the depth of their defect states in the band gap.[18,19] Thus, it is unclear whether predictions of vacancy behavior between the bulk and surfaces in TiO_2 based only on GGA are fully reliable. It is therefore worthwhile to check these results using advanced methods that correct these errors. The simplest method would be to use DFT+U, which includes an on-site repulsion potential U.[20] However, it requires rather unphysical values of U in the case of TiO_2 to give a correct band gap. Thus, it is preferable to use hybrid functional such as B3LYP, the Heyd, Scuseria, Erzernhof (HSE) functional,[21] or screened exchange (sX) functional,[22] which give good representations of the electronic structure. They are also computationally efficient for large supercells of 100−200 atoms needed for defect calculation. The sX hybrid functional method was found to give the accurate band gaps of many semiconductors and insulators and the correct localization of charge near vacancies.[23−27]

Received: March 12, 2015
Revised: July 15, 2015
Published: July 20, 2015

DOI: 10.1021/acs.jpcc.5b02430
J. Phys. Chem. C 2015, 119, 18160−18166

We have previously presented the results for oxygen vacancies in bulk rutile by sX.[28] Similar results using B3LYP, HSE, and GW methods are also available.[18,19,29−33] Here we present the results for the surface oxygen vacancies in TiO_2 by sX. To this end, we calculate the formation energy of oxygen vacancies at three surfaces, anatase (101), reconstructed anatase (001), and rutile (110) by the sX hybrid functional to find out the relative stability of the surface and subsurface positions. In this paper we also include the results of GGA[34] for comparison. It should be noted that B3LYP gives band gaps larger than experiments for rutile,[19] which might have led to stronger defect state localization. Similarly, HSE gives the correct distortions around the bulk O vacancy in rutile. However, the defect level lies at the conduction band edge rather than deeper into the gap as seen experimentally.[29] In contrast, sX gives the correct band gap for rutile and gave the correct vacancy distortions and a deep state for the vacancy.[28]

METHODS

The GGA and screened exchange hybrid functional calculations are carried out using the CASTEP plane wave pseudopotential code.[35] For k sampling we use the Γ point scheme due to the large supercell. The geometry optimization is carried out until the residual force is smaller than 0.01 eV/Å.

The three TiO_2 surfaces we constructed are shown in Figure 1. We used slabs of four TiO_2 layers containing 144 atoms for

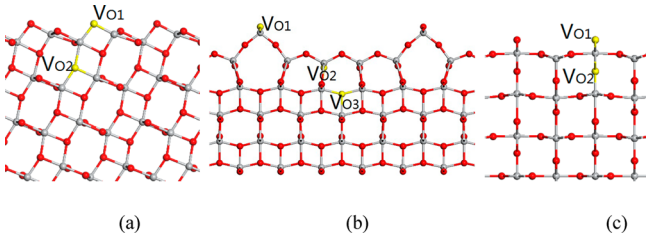

Figure 1. Slab models of (a) the anatase (101) surface, (b) anatase (001) surface, and (c) rutile (110) surface. Oxygen is red; titanium is gray. The various oxygen vacancy sites are yellow.

the anatase (101) surface (2 × 3 surface supercell), and slabs of four TiO_2 layers containing 192 atoms for the rutile (110) surface (4 × 2 surface supercell). For the anatase (001) surface, we took the ADM model[12] as introduced above, with five TiO_2 layers containing 189 atoms (4 × 3 surface supercell). All of the supercell lattice constants are larger than 11 Å in all of the three directions. Our previous study showed that the O vacancy in TiO_2 has strong polaronic effects[36] and thus requires a larger supercell to suppress the defect image interaction.[28] Further calculations of the O vacancy with a larger 3 × 3 × 4 supercell of rutile than in Lee et al.[28] find that the V_O^{+1} state distorts such that the unpaired electron is localized on one of the three adjacent sites, and is therefore in agreement with recent electron spin resonance data.[37] All surfaces were modeled using the periodic boundary conditions with a vacuum of ∼11 Å.

The defect properties are represented by their formation energies as a function of Fermi energy and chemical potential. The charge correction follows Lany and Zunger's scheme.[38] The formation energy H_q of defect with charge q can be calculated by the following expression:[38]

$$H_q(E_F, \mu) = [E_q - E_H] + q(E_V + \Delta E_F) + \sum_\alpha n_\sigma(\mu_\alpha) \quad (1)$$

where E_q and E_H are the total energy of a defect cell and a perfect cell with charge q respectively, ΔE_F is the Fermi level energy with respect to valence band maximum, n_α is the number of atoms of element α, and μ_α is the reference chemical potential of element α. The chemical potentials satisfy the following equation (experimental value):

$$\mu_{Ti} + 2\mu_O = H_f(TiO_2) = -9.73 \text{ eV} \quad (2)$$

The O-rich limit is at $\mu_O = 0$ eV, and $\mu_{Ti} = -9.73$ eV. The O-poor limit (or Ti-rich limit) is not the usual Ti:TiO_2 equilibrium but the Ti_2O_3:TiO_2 equilibrium,[28,29]

$$2\mu_{Ti} + 3\mu_O = H_f(Ti_2O_3) = -15.39 \text{ eV} \quad (3)$$

Therefore, $\mu_O = -H_f(Ti_2O_3) + 2H_f(TiO_2)$ and $\mu_{Ti} = 2H_f(Ti_2O_3) - 3H_f(TiO_2)$, which gives $\mu_O = -4.07$ eV and $\mu_{Ti} = -1.59$ eV.[28]

RESULTS

The local density of states (DOS) of the three kinds of TiO_2 surfaces are shown in the Figure 2 and are compared to the

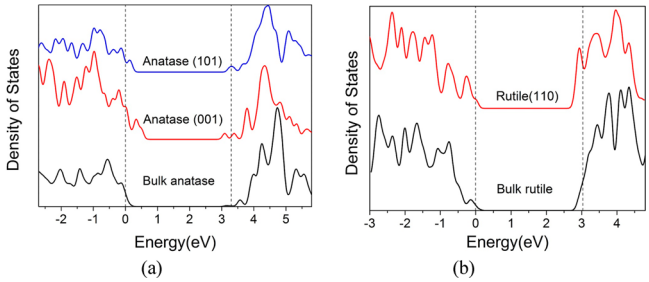

Figure 2. DOS of (a) anatase (101) surface, anatase (001) surface, and bulk anatase; (b) rutile (110) surface and bulk rutile, calculated by the sX-LDA method. The dashed line marks the conduction band minimum and valence band maximum of bulk TiO_2. The O 2s orbital at −20 eV below Fermi level is used as a reference level to align the bulk and interface DOS.

bulk TiO_2 DOS. The calculated bulk TiO_2 band gaps are 3.02 eV for rutile and 3.17 eV for anatase, close to the experimental value. The dangling bonds on the surface introduced the gap states expanding into the band gap of bulk TiO_2. The surface band gaps are thus smaller than the bulk value: 3.11 eV for anatase (101), 2.76 eV for anatase (001), and 2.90 eV for rutile (110). Particularly, in anatase the VBM is shifted up significantly. Our simulation results are consistent with the experimental surface band gap values in previous studies.[39,40]

We have calculated the formation energy of various surface or subsurface neutral oxygen vacancies on all three surfaces in the O-rich condition, as labeled in Figure 1, in both GGA and screened exchange. The most stable ones are listed in Table 1. The formation energy of the oxygen vacancy in bulk TiO_2 is also listed there for comparison.

First we discuss the most stable oxygen vacancies at the anatase (101) surface. The surface defect site V_{O1} corresponds to the removal of an O_{2C}, while V_{O2}, the subsurface defect site, corresponds to the removal of an O_{3C}. Both GGA and sX find that V_{O2} is more favorable, with an energy difference of 0.3 eV for sX and 0.4 eV for GGA. This result is consistent with the quite low surface energy of anatase (101). Thus, it takes more energy to create a *surface* vacancy in anatase. In addition, the subsurface oxygen vacancy formation energy is only 0.17 eV less than that in bulk anatase from sX. Hence the oxygen

DOI: 10.1021/acs.jpcc.5b02430
J. Phys. Chem. C 2015, 119, 18160−18166

Table 1. Formation Energies of Neutral Oxygen Vacancy Defect at Different Sites of Anatase (101), Anatase (001), and Rutile (110) Surfaces[a]

formation energy	vacancy site	GGA (eV)	sX-LDA (eV)
anatase (101)	V_{O1} (surface)	4.37	5.08
	V_{O2} (subsurface)	**3.99**	**4.78**
	V_O in bulk	4.27	4.95
anatase (001)	V_{O1} (surface)	4.74	5.07
	V_{O2} (surface)	4.38	5.12
	V_{O3} (subsurface)	**4.21**	**4.96**
	V_O in bulk	4.27	4.95
rutile (110)	V_{O1} (surface)	**3.71**	**4.39**
	V_{O2} (subsurface)	4.10	4.98
	V_O in bulk	4.79	5.70

[a]Positive value stands for the extra energy needed to form defect. The bold denotes the most stable defect site for each surface. The values are compared with oxygen vacancy in bulk TiO_2. Site labels are given in Figure 1.

vacancy is more likely to form at the anatase (101) subsurface rather than at the surface or bulk site.

We then analyze the three most stable oxygen vacancies on anatase (001). V_{O1} is at the ridge part of the surface, which is originally bonded to two Ti atoms. V_{O2}, corresponding to the removal of an O_{3C}, is at the terrace part of the surface, and V_{O3} is at the subsurface, which is originally bonded to three Ti atoms. Both GGA and sX show that the subsurface oxygen vacancy V_{O3} is most stable, similar to anatase (101). In addition, the formation energy of the oxygen vacancy in bulk anatase is 4.95 eV, which is nearly the same as that of V_{O3} in anatase (001) surface, while the formation energy of V_{O2} in anatase (101) is 0.2 eV smaller. Thus, the subsurface oxygen vacancy in anatase (001) experiences an environment similar to the bulk TiO_2, and the oxygen vacancy is likely to form at subsurface and bulk site rather than surface. Furthermore, we can also conclude that O vacancies slightly prefer to form at the subsurface rather than the top surface of anatase (101) and (001).

For rutile (110), Table 1 lists the two most stable oxygen vacancies that we find in our calculations. V_{O1} is at the surface, which is originally bonded to two Ti atoms, while V_{O2} is a subsurface defect corresponding to the removal of an O_{3C} atom. Both GGA and sX show that V_{O1} is the most stable defect with a formation energy of 1.3 eV lower than V_O in bulk rutile. Thus, oxygen vacancies are more likely to form at the rutile surface. This result can be interpreted as that it is only necessary to break two Ti−O bonds to create an oxygen vacancy at the rutile (110) surface rather than to break three Ti−O bonds at subsurface or bulk. This is quite different from anatase (101) or (001) where the subsurface defect is quite similar to the bulk case.

Removal of an oxygen atom in the TiO_2 surface structure creates two unpaired electrons (for the neutral defect) and dangling bonds on adjacent Ti atoms. Figure 3a shows that on the anatase (101) surface removal of the oxygen atom at V_{O2} shifts the adjacent Ti atoms away from the defect and nearby oxygen atoms toward the defect. The Ti−Ti distance increases from 3.20 to3.70 Å and from 4.00 to4.75 Å and a Ti−O bond near the defect breaks due to the distortion. Figure 3b shows that on anatase (001) surface the removal of an oxygen atom at the V_{O3} site also causes adjacent Ti atoms to move apart and O atoms to move closer to defect. The Ti−Ti distance between

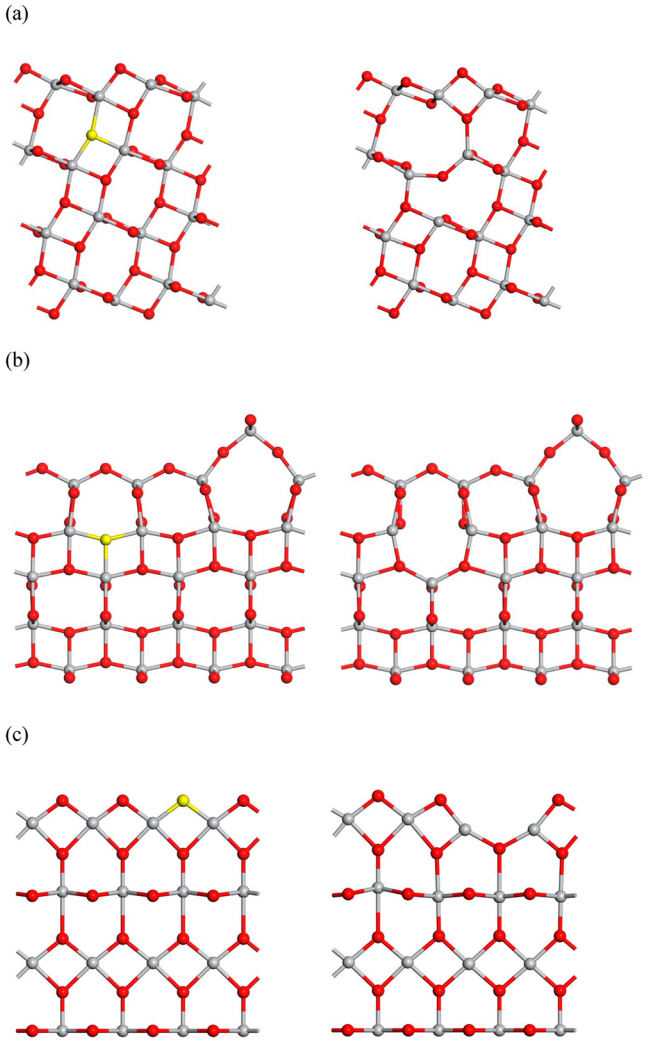

Figure 3. Side view of atomic spacing of (a) anatase (101) surface, (b) anatase (001) surface and (c) rutile (110) surface. The figures on the left are perfect slabs without defect, and the figures on the right are the surface structure with an oxygen vacancy after geometry relaxation.

adjacent Ti atoms increases from 3.77 to4.12 Å and from 3.08 to3.43 Å and the O−O distance between nearby O atoms decrease from 3.74 to3.34 Å. Figure 3c shows that for the rutile (110) surface, the lowest cost O vacancy is at the surface. Removing an oxygen atom only forms two Ti dangling bonds. This not only causes the adjacent Ti atoms to move away from defect, increasing the separation from 2.96 to3.37 Å, but also triggers these two Ti atoms to move 0.40 Å downward into bulk. However, the next-nearest Ti atoms stay nearly unchanged, thus the oxygen vacancy only leads to a local deformation in TiO_2.

Figure 4 shows the calculated formation energies of most stable oxygen vacancies at these three surfaces for both O-poor and O-rich conditions by sX, as a function of the Fermi energy. Defect charge states from −2 to 2 have been calculated. Possible spin polarization is also included. The E_C and E_V here refer to the conduction band and valence band edge of the TiO_2 surface system. The surface band gap is smaller than bulk value. The charge transition levels correspond to the Fermi energy at which the charge q and q' defect states have the same formation energy. The defect charge state would change at these energies.

DOI: 10.1021/acs.jpcc.5b02430
J. Phys. Chem. C 2015, 119, 18160−18166

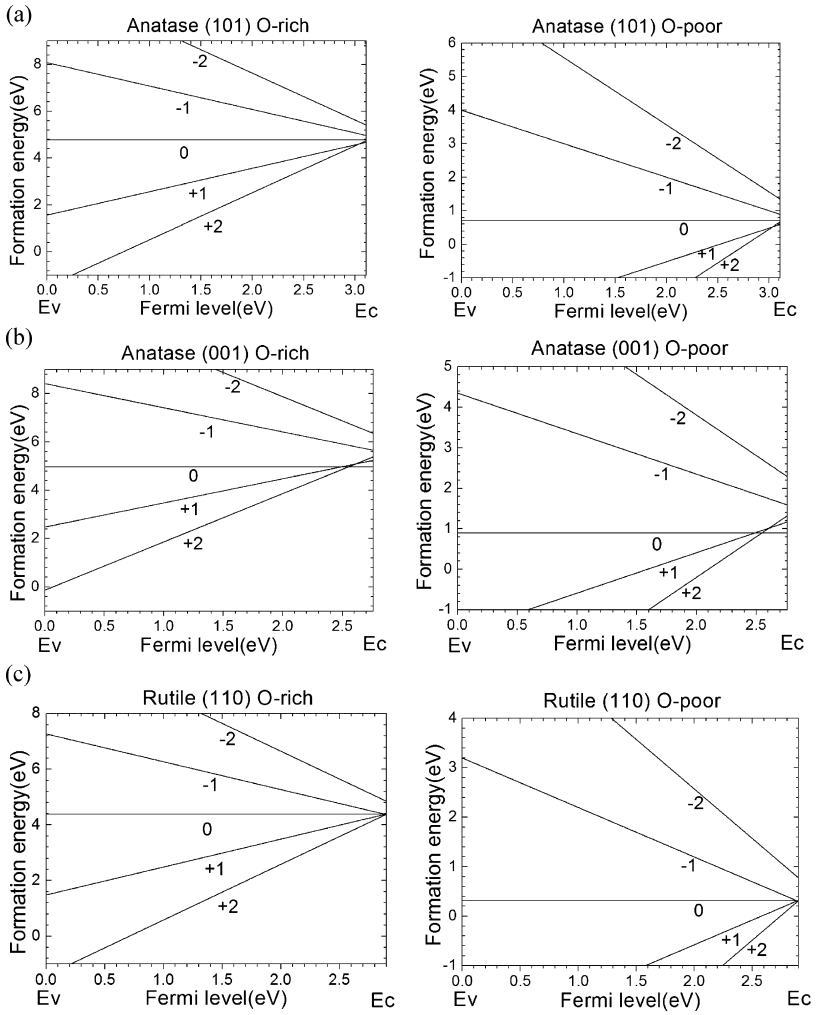

Figure 4. Oxygen vacancy formation energy against Fermi level at O-rich and O-poor conditions, calculated by sX-LDA for (a) anatase (101), (b) anatase (001), and (c) rutile (110) surface. E_C and E_V refer to the conduction band and valence band edge of TiO_2 surface. Negative charge states are also shown for completeness.

On the anatase (101) surface, the most stable oxygen vacancy V_{O2} is mostly dominated by the +2 charge state, and the calculated V_O^{+}/V_O^{2+} charge transition is just 0.1 eV below the surface conduction band minimum (CBM). At the O-rich limit, the formation energy of V_O^{0} is 4.60 eV. On the anatase (001) surface, the formation energy of V_{O3}^{0} is 4.96 eV when E_F is near the conduction band edge. The V_O^{0}/V_O^{2+} charge transition is at 0.2 eV below the conduction band. The +1 charge state is unstable. So it is a negative U system.[41] For the rutile (110) surface, the most stable surface defect V_{O1}^{0} has the formation energy of 4.39 eV when E_F is near the conduction band edge, while the 2+ charge state is most stable for E_F lying lower in the band gap.

Figure 5 shows the partial density of states (PDOS) of the most stable defect sites for V_O^{2+} charge state on the three surfaces. Here we compared the total DOS, the PDOS on Ti atoms near defect and in the bulk, as well as the PDOS on O atoms in bulk. In sX, the oxygen vacancy gives rise to a defect state just above CBM on anatase (101) and anatase (001) surface, while a defect state appears below CBM on rutile (110) surface.

The charge density for V_{O2}^{0}, V_{O2}^{+}, and V_{O2}^{2+} defects on anatase (101) are shown in Figure 6a–c, respectively, from the same direction. Different charge states of the defect trigger different lattice distortions on adjacent sites. Interestingly, the charge density is localized on two Ti atoms rather than the defect site. One of the Ti atoms is the nearest neighbor, and the other is the next-nearest neighbor. Both of them are at the surface. This is different from that in bulk TiO_2 as described in ref 28 due to the influence of the surface. However, this localization scheme is consistent with the B3LYP and PBE+U results of Di Valentin et al.[19] Recent studies on the anatase (101) surface show that the surface-induced 5-fold Ti can introduce a strong polaronic effect and localize the excess electrons near the surface.[42,43] We have also calculated the charge density of defect level on anatase (001) and rutile (110) surface. Both of them are delocalized and not shown here.

DISCUSSION

Various experimental studies have confirmed the existence of oxygen vacancies on the surface of rutile (110), which are in good agreement with our simulation results. Fukui et al.[9] directly observed the oxygen vacancies on rutile (110) surface by AFM. Wendt et al.[10] also confirmed the existence of oxygen vacancies on this surface by STM. Both AFM and STM figures of surface oxygen vacancies support our simulation results that oxygen vacancies are more likely to form on the surface of rutile (110), since the formation energy of the oxygen vacancy at

DOI: 10.1021/acs.jpcc.5b02430
J. Phys. Chem. C 2015, 119, 18160−18166

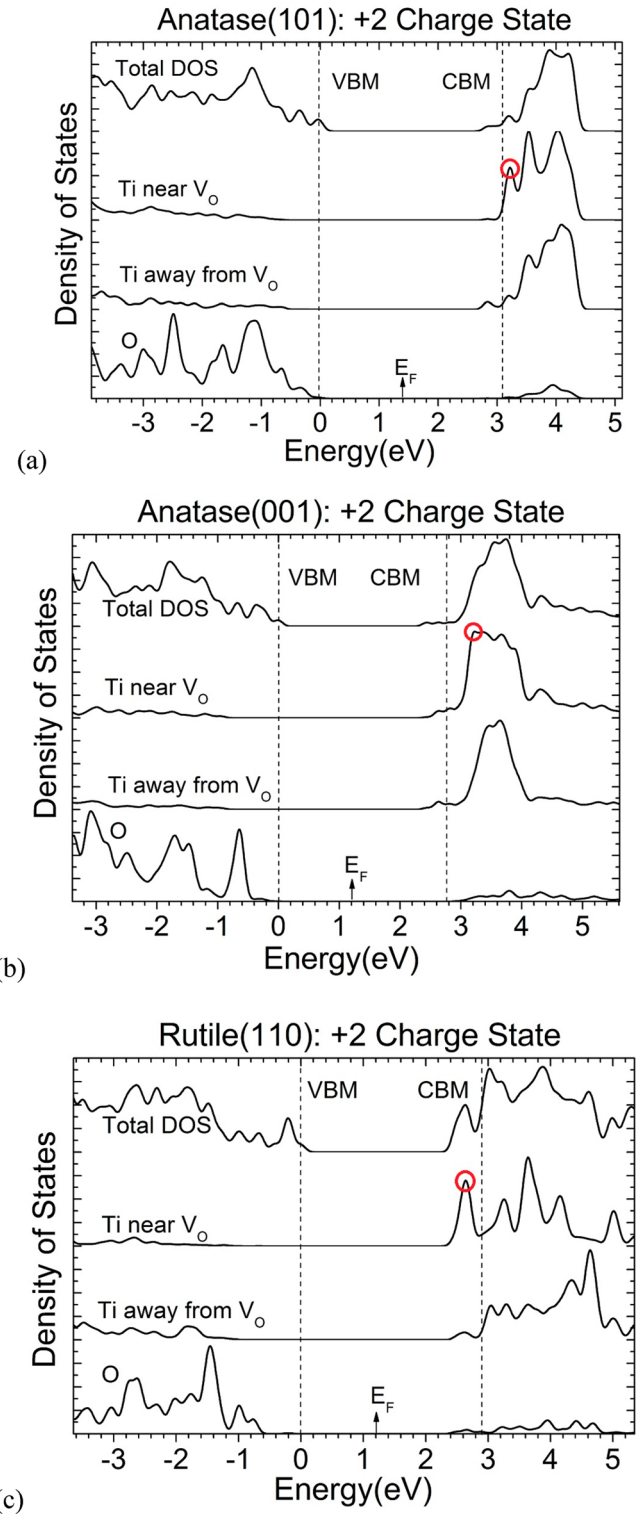

Figure 5. Partial density of states (PDOS) of the three TiO_2 surfaces with an oxygen vacancy at +2 charge states, (a) anatase (101) surface, (b) anatase (001) surface, and (c) rutile (110) surface, by sX-LDA method. The PDOS on a Ti atom near the defect, on a Ti atom away from defect, and on an O atom are shown here and compared with total DOS. The VBM and CBM are calculated from the perfect surface slab model and aligned to the PDOS of the defect system. The defect peak is indicated with a red circle in each figure.

rutile (110) surface is smaller than that at the subsurface and much smaller than that in bulk rutile.

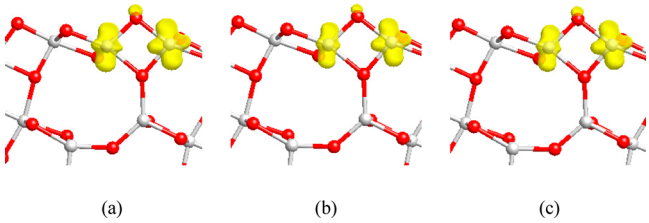

Figure 6. Charge density contour for oxygen vacancy near CBM of anatase (101) surface: (a) V_{O2}^{0}, (b) V_{O2}^{+}, and (c) V_{O2}^{2+}.

We compare our sX simulation results of the neutral V_O formation energy with the GGA results by Cheng et al.[15] Both GGA and sX show that subsurface V_O is the most stable for the two anatase surfaces, while the surface V_O is the most stable for rutile (110) surfaces.

We also take larger supercells for all three surface models than in Cheng et al.[15] In our simulation, a distance of at least 10 Å is ensured between the defect and its image in all directions, and the slab model is thick enough along z direction to eliminate the influence of the bottom surface. Our cell size tests indicate that a smaller supercell can lead to an incorrect order of formation energies. For the anatase (001) surface, the four slabs supercell we have tested is not thick enough that the subsurface V_{O3} could be influenced by both the top surface and the bottom surface in the model, which results in an unreasonable charge distribution and formation energy.

We also compare our results of V_O on the surface and in the bulk with other advanced methods beyond GGA such as GW. It is widely agreed that the neutral V_O formation energy in bulk rutile at O-poor limit is around 1.8 eV, which is also confirmed by our simulation. However, the +2 charge state of V_O formation energy differs largely in different work. In O-poor condition when Fermi level is at the VBM, the HSE result given by Janotti et al.[29] suggests this value to be −5.1 eV, while the GW result of Malashevich et al.[30] gives the formation energy of −3.7 eV. Our sX results give −4.30 eV, which is in the reasonable region. By comparing the oxygen vacancy formation energy on the surface and in the bulk, we find that anatase has a similar formation of V_O on surface as it is in bulk, while rutile V_O on the surface is thermodynamically much preferred than in bulk V_O. Thus, V_O is likely to form in the surface area, while for the anatase surface the oxygen vacancy tends to form at the subsurface and bulk region.

Our simulation also shows that formation energy of oxygen vacancy at anatase (101) subsurface is smaller than that at anatase (001). The O vacancy formation probability is roughly the same for all sites (including the surface ones) with only slight preference for subsurface or bulk regions of anatase(101) or (001) surfaces. So the surface and subsurface region does not possess any advantage over bulk for the oxygen vacancy's formation. These two mechanisms jointly explain the reason for a much lower oxygen vacancy concentration on the anatase (001) surface than the anatase (101) surface as indicated by resonant photoemission data.[14]

It is also interesting to use our results for interpreting oxygen vacancy behavior in RRAM. In this case, a scavenging metal layer is usually included, so that the system is in the O poor limit. In addition, the electrode metals are chosen to set the resting Fermi energy. E_F will tend to lie in the range of 4.3 to 5.3 eV below vacuum, or 0.4−1.4 eV below the bulk conduction band edge. In the O-poor limit, the neutral O vacancy formation energy becomes quite low, below 1 eV.

DOI: 10.1021/acs.jpcc.5b02430
J. Phys. Chem. C 2015, 119, 18160−18166

When E_F is lowered to that the vacancy enters its 2+ charge state, its formation energy becomes negative. The Fermi level cannot move further toward the lower part of band gap.[44] This is indeed what happens in the devices, and the vacancies then coalesce to form the conductive filament.

CONCLUSIONS

We calculate the electronic structure of oxygen vacancies with different charge states on three TiO_2 by screened exchange functional. On all of the three surfaces, the +2 charge state is the most stable for oxygen vacancy in most part of band gap. The formation energy of V_O is negative near VBM at O-rich limit so that O vacancy could form spontaneously at low Fermi level or O poor condition. This is favorable to the formation of the conducting channel in RRAM. The energy differences among various sites are small in anatase with slightly preference for subsurface, while the rutile surface site has much lower formation energy. For all three TiO_2 surface models, oxygen vacancies introduce a gap state near the conduction band edge. The defect orbital is localized on a neighboring Ti atom and a next-nearest Ti atom, which is different from a bulk TiO_2 defect.

AUTHOR INFORMATION

Notes

The authors declare no competing financial interest.

REFERENCES

(1) Diebold, U. The Surface Science of Titanium Dioxide. *Surf. Sci. Rep.* **2003**, *48*, 53−229.

(2) Asahi, R.; Morikawa, T.; Ohwaki, T.; Aoki, K.; Taga, Y. Visible-light Photocatalysis in Nitrogen-doped Titanium Oxides. *Science* **2001**, *293*, 269−271.

(3) Gratzel, M. Photoelectrochemical Cells. *Nature* **2001**, *414*, 338−344.

(4) Kwon, D. H.; Kim, K. M.; Jang, J. H.; Jeon, J. M.; Lee, M. H.; Kim, G. H.; Li, X. S.; Park, G. S.; Lee, B.; Han, S.; et al. Atomic Structure of Conducting Nanofilaments in TiO_2 Resistive Switching Memory. *Nat. Nanotechnol.* **2010**, *5*, 148−153.

(5) Yim, C. M.; Pang, C. L.; Thornton, G. Oxygen Vacancy Origin of the Surface Band-Gap State of TiO_2 (110). *Phys. Rev. Lett.* **2010**, *104* (3), 036806.

(6) Schaub, R.; Thostrup, P.; Lopez, N.; Laegsgaard, E.; Stensgaard, I.; Norskov, J. K.; Besenbacher, F. Oxygen Vacancies as Active Sites for Water Dissociation on Rutile TiO_2(110). *Phys. Rev. Lett.* **2001**, *87*, 266104.

(7) Park, S. G.; Magyari-Kope, B.; Nishi, Y. Impact of Oxygen Vacancy Ordering on the Formation of a Conductive Filament in TiO_2 for Resistive Switching Memory. *IEEE Electron Device Lett.* **2011**, *32*, 197−199.

(8) Guo, Y.; Robertson, J. Materials Selection for Oxide-Based Resisitive Random Access Memories. *Appl. Phys. Lett.* **2014**, *105*, 223516.

(9) Fukui, K.; Onishi, H.; Iwasawa, Y. Atom-resolved Image of the TiO_2(110) Surface by Noncontact Atomic Force Microscopy. *Phys. Rev. Lett.* **1997**, *79*, 4202−4205.

(10) Wendt, S.; Schaub, R.; Matthiesen, J.; Vestergaard, E. K.; Wahlstrom, E.; Rasmussen, M. D.; Thostrup, P.; Molina, L. M.; Laegsgaard, E.; Stensgaard, I.; et al. Oxygen Vacancies on TiO_2(110) and their Interaction with H_2O and O_2: A Combined High-resolution STM and DFT Study. *Surf. Sci.* **2005**, *598*, 226−245.

(11) Ranade, M. R.; Navrotsky, A.; Zhang, H. Z.; Banfield, J. F.; Elder, S. H.; Zaban, A.; Borse, P. H.; Kulkarni, S. K.; Doran, G. S.; Whitfield, H. J. Energetics of Nanocrystalline TiO_2. *Proc. Natl. Acad. Sci. U. S. A.* **2002**, *99*, 6476−6481.

(12) Lazzeri, M.; Selloni, A. Stress-driven Reconstruction of an Oxide Surface: The Anatase TiO_2 (001)-(1 × 4) Surface. *Phys. Rev. Lett.* **2001**, *87*, 266105.

(13) Yang, H. G.; Sun, C. H.; Qiao, S. Z.; Zou, J.; Liu, G.; Smith, S. C.; Cheng, H. M.; Lu, G. Q. Anatase TiO_2 Single Crystals with a Large Percentage of Reactive Facets. *Nature* **2008**, *453*, 638−641.

(14) Thomas, A. G.; Flavell, W. R.; Mallick, A. K.; Kumarasinghe, A. R.; Tsoutsou, D.; Khan, N.; Chatwin, C.; Rayner, S.; Smith, G. C.; Stockbauer, R. L.; et al. Comparison of the Electronic Structure of Anatase and Rutile TiO_2 Single-crystal Surfaces Using Resonant Photoemission and X-Ray Absorption Spectroscopy. *Phys. Rev. B: Condens. Matter Mater. Phys.* **2007**, *75*, 035105.

(15) Cheng, H. Z.; Selloni, A. Surface and Subsurface Oxygen Vacancies in Anatase TiO_2 and Differences with Rutile. *Phys. Rev. B: Condens. Matter Mater. Phys.* **2009**, *79*, 092101.

(16) Mori-Sanchez, P.; Cohen, A. J.; Yang, W. T. Localization and Delocalization Errors in Density Functional Theory and Implications for Band-gap Prediction. *Phys. Rev. Lett.* **2008**, *100*, 146401.

(17) Pacchioni, G. Modeling Doped and Defective Oxides in Catalysis with Density Functional Theory Methods: Room for Improvements. *J. Chem. Phys.* **2008**, *128*, 182505.

(18) Di Valentin, C.; Pacchioni, G.; Selloni, A. Electronic Structure of Defect States in Hydroxylated and Reduced Rutile TiO_2(110) surfaces. *Phys. Rev. Lett.* **2006**, *97*, 166803.

(19) Di Valentin, C.; Pacchioni, G.; Selloni, A. Reduced and n-Type Doped TiO_2: Nature of Ti^{3+} Species. *J. Phys. Chem. C* **2009**, *113*, 20543−20552.

(20) Morgan, B. J.; Watson, G. W. A DFT + *U* Description of Oxygen Vacancies at the TiO_2 Rutile (1 1 0) Surface. *Surf. Sci.* **2007**, *601*, 5034−5041.

(21) Heyd, J.; Scuseria, G. E.; Ernzerhof, M. Hybrid Functional based on a Screened Coulomb Potential. *J. Chem. Phys.* **2003**, *118*, 8207−8215.

(22) Bylander, D. M.; Kleinman, L. Good Semiconductor Band-Gaps with a Modified Local-Density Approximation. *Phys. Rev. B: Condens. Matter Mater. Phys.* **1990**, *41*, 7868−7871.

(23) Clark, S. J.; Robertson. Screened Exchange Density Functional Applied to Solids. *Phys. Rev. B: Condens. Matter Mater. Phys.* **2010**, *82*, 085208.

(24) Guo, Y.; Clark, S. J.; Robertson, J. Calculation of Metallic and Insulating Phases of V_2O_3 by Hybrid Density Functionals. *J. Chem. Phys.* **2014**, *140*, 054702.

(25) Guo, Y.; Robertson, J.; Clark, S. J. The Effects of Screening Length in the Non-local Screened-exchange Functional. *J. Phys.: Condens. Matter* **2015**, *27*, 025501.

(26) Gillen, R.; Robertson, J. Hybrid Functional Calculations of the Al Impurity in α Quartz: Hole Localization and Electron Paramagnetic Resonance Parameters. *Phys. Rev. B: Condens. Matter Mater. Phys.* **2012**, *85*, 014117.

(27) Gillen, R.; Clark, S. J.; Robertson, J. Nature of the Electronic Band Gap in Lanthanide Oxides. *Phys. Rev. B: Condens. Matter Mater. Phys.* **2013**, *87*, 125116.

(28) Lee, H. Y.; Clark, S. J.; Robertson, J. Calculation of Point Defects in Rutile TiO_2 by the Screened-Exchange Hybrid Functional. *Phys. Rev. B: Condens. Matter Mater. Phys.* **2012**, *86*, 075209.

(29) Janotti, A.; Varley, J. B.; Rinke, P.; Umezawa, N.; Kresse, G.; Van de Walle, C. G. Hybrid Functional Studies of the Oxygen Vacancy in TiO_2. *Phys. Rev. B: Condens. Matter Mater. Phys.* **2010**, *81*, 085212.

(30) Malashevich, A.; Jain, M.; Louie, S. G. First-principles DFT Plus GW Study of Oxygen Vacancies in Rutile TiO_2. *Phys. Rev. B: Condens. Matter Mater. Phys.* **2014**, *89*, 075205.

(31) Zhanpeisov, N. U.; Fukumura, H. Oxygen Vacancy Formation on Rutile TiO_2 (110) and its Interaction with Molecular Oxygen: A Theoretical Density Functional Theory Study. *J. Phys. Chem. C* **2007**, *111*, 16941−16945.

(32) Ortega, Y.; Hevia, D. F.; Oviedo, J.; San-Miguel, M. A. A DFT Study of the Stoichiometric and Reduced Anatase (001) Surfaces. *Appl. Surf. Sci.* **2014**, *294*, 42−48.

DOI: 10.1021/acs.jpcc.5b02430
J. Phys. Chem. C 2015, 119, 18160−18166

(33) Zhu, L. G.; Hu, Q. M.; Yang, R. The Effect of Electron Localization on the Electronic Structure and Migration Barrier of Oxygen Vacancies in Rutile. *J. Phys.: Condens. Matter* **2014**, *26*, 055602.
(34) Perdew, J. P.; Burke, K.; Ernzerhof, M. Generalized Gradient Approximation Made Simple. *Phys. Rev. Lett.* **1996**, *77*, 3865−3868.
(35) Clark, S. J.; Segall, M. D.; Pickard, C. J.; Hasnip, P. J.; Probert, M. J.; Refson, K.; Payne, M. C. First Principles Methods Using CASTEP. *Z. Kristallogr.* **2005**, *220*, 567−570.
(36) Deák, P.; Aradi, B.; Frauenheim, T. Polaronic Effects in TiO_2 Calculated by the HSE06 Hybrid Functional: Dopant Passivation by Carrier Self-trapping. *Phys. Rev. B: Condens. Matter Mater. Phys.* **2011**, *83*, 155207.
(37) Brant, A. T.; Giles, N. C.; Halliburton, L. E. Insertion of Lithium ions into TiO_2 (rutile) Crystals: An Electron Paramagnetic Resonance Study of the Li-associated Ti^{3+} Small Polaron. *J. Appl. Phys.* **2013**, *113*, 053712.
(38) Lany, S.; Zunger, A. Assessment of Correction Methods for the Band-gap Problem and for Finite-size Effects in Supercell Defect Calculations: Case Studies for ZnO and GaAs. *Phys. Rev. B: Condens. Matter Mater. Phys.* **2008**, *78*, 235104.
(39) Goniakowski, J.; Noguera, C. Electronic-Structure of Clean Insulating Oxide Surfaces 0.1. A Numerical Approach. *Surf. Sci.* **1994**, *319*, 68−80.
(40) Majumder, S.; Paramanik, D.; Solanki, V.; Bag, B. P.; Varma, S. Bandgap Tailoring of Rutile TiO_2(110) via Surface Patterning with Electron Cyclotron Resonance Sputtering. *Appl. Phys. Lett.* **2011**, *98*, 053105.
(41) Baraff, G. A.; Kane, E. O.; Schluter, M. Theory of the Silicon Vacancy - an Anderson Negative-U System. *Phys. Rev. B: Condens. Matter Mater. Phys.* **1980**, *21*, 5662−5686.
(42) Setvin, M.; Franchini, C.; Hao, X.; Schmid, M.; Janotti, A.; Kaltak, M.; Van de Walle, C. G.; Kresse, G.; Diebold, U. Direct View at Excess Electrons in TiO_2 Rutile and Anatase. *Phys. Rev. Lett.* **2014**, *113*, 086402.
(43) Deák, P.; Kullgren, J.; Frauenheim, T. Polarons and oxygen vacancies at the surface of anatase TiO_2. *Phys. Status Solidi RRL* **2014**, *8*, 583−586.
(44) Robertson, J.; Clark, S. J. Limits to Doping in Oxides. *Phys. Rev. B: Condens. Matter Mater. Phys.* **2011**, *83*, 075205.

DOI: 10.1021/acs.jpcc.5b02430
J. Phys. Chem. C 2015, 119, 18160−18166